Applied Catalysis B: Environmental 134–135 (2013) 359–366

Contents lists available at SciVerse ScienceDirect

Applied Catalysis B: Environmental

journal homepage: www.elsevier.com/locate/apcatb

Autothermal steam reforming of ethanol over $La_2Ce_{2-x}Ru_xO_7$ ($x = 0$–0.35) catalyst for hydrogen production

Sheng-Feng Weng, Yun-Hsin Wang, Chi-Shen Lee*

Department of Applied Chemistry, National Chiao Tung University, 1001 Daxue Rd., Hsinchu 30010, Taiwan

ARTICLE INFO

Article history:
Received 24 April 2012
Received in revised form
17 December 2012
Accepted 8 January 2013
Available online 29 January 2013

Keywords:
Autothermal steam reforming of ethanol
Pyrochlore
Solid solution
Ruthenium

ABSTRACT

Pyrochlore phases solid solutions, $La_2Ce_{2-x}Ru_xO_7$ ($x = 0$–0.35) were prepared with a sol–gel process and used as catalysts for the autothermal steam reforming of ethanol. The samples as prepared were characterized with powder X-ray diffraction (PXRD), X-ray photoelectron spectra (XPS), and temperature-programmed reduction (TPR). The XPS and TPR spectra revealed the effect of doped Ru^{n+} to oxidation states of La and Ce sites. The low temperature reduction ability and relative concentration of Ce^{4+} ions are increased as the cell-dimension decreased. Tests of catalytic activity showed that the reforming performance of $La_2Ce_{2-x}Ru_xO_7$ catalysts was affected by the Ru/Ce loading ratio. For all catalysts, partial oxidation was favored at a large C/O composition; incomplete ethanol conversion was observed for C/O ≥ 0.7. The optimized catalyst was $La_2Ce_{1.8}Ru_{0.2}O_7$ with hydrogen production rate (r_{H_2}) 2.01×10^{-3} mol s^{-1} g_{cat}^{-1} (autothermal temperature ~600 °C and 97% ethanol conversion at C/O = 0.6). The catalyst exhibited stable r_{H_2} over 26 h of the reaction with ethanol conversion >95%. r_{H_2} of the catalyst gradually decreased thereafter because $LaAlO_3$ started to formed and affected catalytic process. For the catalyst, the Ru ions remained well dispersed before and after the AESR reaction.

1. Introduction

Global warming, a critical topic, draws much attention. The burning of fossil fuels is accompanied by the production of pollutants such as CO_x, NO_x, CH_x and SO_x that cause severe influence to our surroundings; including the greenhouse effect. Although fossil fuels are the major energy source of the world, providing ~80% of our daily power supply, they have limited availability in nature and will become severely depleted in the mid-21st century. Scientists have hence devoted effort to investigate renewable sources of energy to solve a prospective crisis. Among these available sources, hydrogen is a prospective carrier of energy because of its content of energy per unit mass (i.e., 120.7 kJ/g) is larger than for other fuels; it burns cleanly without emitting pollutants to our environment [1,2].

Hydrogen gas produced by ethanol reforming is considered to be a sustainable process [3–5]. The overall reaction can be depicted stoichiometrically as:

$$C_2H_5OH + 3H_2O \rightarrow 3CO_2 + 6H_2, \quad \Delta H^{o}_{298} = +347.4\ \text{kJ/mol} \qquad (1)$$

An alternative conversion of ethanol into H_2 is autothermal steam reforming (AESR). In this process, mixtures of ethanol, water, and O_2 gases are injected in a specific proportion; H_2 is thereby produced exothermically [4–6]. The overall reaction can be derived as

$$C_2H_5OH + 2H_2O + \frac{1}{2}O_2 \rightarrow 2CO_2 + 5H_2, \quad \Delta H_R \approx -50\ \text{kJ/mol} \qquad (2)$$

According to this reforming, H_2 (5 mol) is produced from ethanol (1 mol) with ideal selectivity $S_{H_2} = 167\%$. Schmidt's group reported an effective rhodium–ceria catalyst that promoted AESR to produce H_2 from ethanol in a large yield [6]. Ceria is well known for its excellent catalytic activity in various reactions [7–10], such as its satisfactory oxidative ability and capacity for storage of oxygen ions, through the facile transformation between Ce^{3+} and Ce^{4+} ions [11]. The morphology of ceria nanocrystals influences the catalytic activity, and catalytic activity for ethanol reformation depends on crystal facets, but ceria nanocrystals with specially exposed facets exhibit unstable activity and the nanostructures collapse after testing for 24 h [12]. Research on ceria has also focused on the effects of crystal defects. In our preceding work we developed solid solutions of ceria nanocrystals $Ce_{1-x}M_xO_2$ (M = Ti, Zr, and Hf) with controlled morphologies; an analysis of hydrogen temperature-programmed reduction (H_2-TPR) revealed the direct effect of the crystal defects on reductive ability [13,14].

The pyrochlore phase is understood as a defect structure of fluorite type with general formula $A_2B_2O_6$ or $A_2B_2O_7$. This structure exhibits *ccp* arrays of cations with anions partially occupying the tetrahedral sites to form a distorted structure containing intrinsic

* Corresponding author. Tel.: +886 3 5131332; fax: +886 3 5723764.
E-mail addresses: chishen@mail.nctu.edu.tw, chishenlee@gmail.com (C.-S. Lee).

0926-3373/$ – see front matter © 2013 Elsevier B.V. All rights reserved.
http://dx.doi.org/10.1016/j.apcatb.2013.01.025

defects [15,16]. According to the structural features of a pyrochlore phase, the B site in a pyrochlore structure has six-coordination with interatomic distances in a range 1.8∼2.3 Å, which is suitable for substitution by transition-metal cations [17,18]. Besides, the peculiar cation alignment in pyrochlore structure also implies potential catalytic applications [19–21].

Research on pyrochlore material has been focused on applications such as catalytic [17,22–24], electronic [25], optical [26] magnetic properties [27] and SOFC electrode materials [28]; there is no report of pyrochlore materials as catalyst for an steam reforming of ethanol. In this work, we have prepared, through sol–gel methods, Ru-doped pyrochlore phases, $La_2Ce_{2-x}Ru_xO_7$ (x = 0–0.35), in a series to assess their catalytic performance. Doping Ru ions into $La_2Ce_2O_7$ structure is expected to create further crystal defects and to improve the activity in an AESR reaction. Otherwise, the preparation of solid solutions might also avoid the catalytic deactivation caused by the formation and vaporization of gaseous $RuO_{3\,(g)}$ and $RuO_{4\,(g)}$ [29]. AESR performance is tested; the results correlate well with their chemical properties characterized by powder X-ray diffraction (PXRD), temperature-programmed reduction (TPR), and X-ray photoelectron spectra.

2. Experiments

2.1. Synthesis

All reactions were conducted with wet chemical routes. Metal nitrates and metal oxides served as sources of metal ions. All chemicals had analytical grade and were used without further purification.

The sol–gel method was applied to synthesize Ru-doped pyrochlore samples. In a typical experiment, poly(ethandiol)-block-poly(propandiol)-block-poly(ethandiol) copolymer, $HO(CH_2CH_2O)_{20}(CH_2CH(CH_3)O)_{70}(CH_2CH_2O)_{20}H$ (designated $EO_{20}PO_{70}EO_{20}$; Pluronic 123; Aldrich, 1 g) was dissolved in ethanol (10 g) and served as a surfactant. $La(NO_3)_3{\cdot}6H_2O$, $Ce(NO_3)_3{\cdot}6H_2O$, and $RuCl_3{\cdot}xH_2O$ were added in quantitative proportions according to La, Ce, and Ru ions in fixed stoichiometries to 5 mmol in total. After stirring for at least 1 h, the resulting sol solution was gelled at 40 °C in air for 3 days, during which the surfactant P123 polymerized and metal oxide was formed in a network. The surfactant species was then removed on calcining the samples as made at 900 °C for 5 h. For comparison, metal oxide CeO_2 was prepared with the same procedure.

2.2. Preparation of the catalyst

2.2.1. Preparation of $La_2Ce_{2-x}Ru_xO_7$ (x = 0–0.35)

Catalysts were prepared with conventional impregnation. In a general procedure, the metal oxides (0.1 g) as made were well dispersed in ethanol (∼3 mL) in appropriate proportions with an ultrasonic treatment (MICROSONTM XL 2000). Alumina of large specific surface area (corundum; 18 mesh; 1 g; S_{BET} > 300 m^2/g) was then immersed in that solution as the supporting material. The solvent was dried at 80 °C; the entire procedure was repeated at least five times to yield metal oxides well dispersed on the Al_2O_3 support. The catalysts as prepared were then used to test the AESR without further treatment.

2.2.2. Preparation of 5% Ru/CeO_2 and 5% $Ru/La_2Ce_2O_7$ catalysts

The catalysts of 5% Ru/CeO_2 and 5% $Ru/La_2Ce_2O_7$ were dispersed on Al_2O_3 supports according to the process described in 2.2.1. Metal oxide (0.1 g), CeO_2 and $La_2Ce_2O_7$ were first supported on Al_2O_3; the $RuCl_3{\bullet}xH_2O$ solution was then added. The loaded proportions of Ru metal were maintained at ∼5 mass % of the metal oxide. Before the AESR tests, the catalysts as made were reduced under flowing H_2 (0.2 SLPM, 600 °C, 5 h) to activate the catalysts.

2.3. Characterization

2.3.1. Powder X-ray diffraction

Powder X-ray diffraction (PXRD) data for the products were measured at 295 K on a powder diffractometer (Bruker D8 Advance Bragg–Brentano-type, 40 kV, 40 mA, Cu Kα, λ = 0.15418 nm). For phase identification, XRD data were collected in a range 2θ from 20° to 80° with a step interval 0.02°.

2.3.2. Scanning electron microscopy and energy-dispersive spectra

The morphologies of products were examined with a scanning electron microscope (JEOL JSM-7401F FE-SEM). The images were acquired with accelerating voltage 10 kV with several magnifications. Semiquantitative microprobe analysis was performed with an energy-dispersive spectral detector (Oxford INCA Energy 350) equipped on the SEM.

2.3.3. X-ray photoelectron spectra

To examine the oxidation states of each element, we recorded (PHI Quantera SXM instrument, scanning monochromatic X-radiation, Al anode) X-ray photoelectron spectra of C1*s*, O1*s*, Ru3*d*, La3*d* and Ce3*d* core levels. The pressure in the chamber was less than 6.7×10^{-7} Pa during the experiment. All spectra were fitted with a XPS peak software package.

2.3.4. Temperature-programmed reduction

Temperature-programmed reduction (TPR) was performed in a quartz microreactor (China Chromatography 660 instrument, thermal-conductivity detector, TCD). A sample (approximately 80 mg) was loaded into a silica tube and sealed with silica wool. The sample was heated to 900 °C at a rate 10 °C/min in a reducing atmosphere (10% H_2 in flowing Ar).

2.3.5. Specific surface areas

N_2 adsorption–desorption measurements were performed at 77 K using Micrometrics sorptometer Tri Star 3000. The specific surface areas (SSA) of samples were estimated by the Brunauer–Emmet–Teller (BET) method. Prior to the sorption measurement, the samples were degassed at 473 K overnight.

2.4. Measurement of catalytic performance

The autothermal ethanol steam reforming reactions were carried out in a quartz fixed-bed reactor with the inner diameter ∼4 mm, and length ∼12 cm. The 1.5 cm catalytic specimen was loaded and the gas hourly space velocity (GHSV) was maintained at 1.6×10^5 h^{-1}. An HPLC pump was equipped to feed the fuels containing a water/ethanol mixture of known composition (molar ratio of H_2O:C_2H_5OH = 3:1). The feeding amount of water/ethanol mixture was in terms of the carbon-to-oxygen ratio (C/O); a factor that would affect the oxidation process of fuels, and could be defined by the following equation [6,30]:

$$\mathrm{C/O} = \frac{\text{mole of C of inlet fuels}}{\text{mole of O of inlet fuels exclude } H_2O}$$

A three-zone heating furnace was used to control the temperature of vaporization of the water/ethanol mixture and the preheating temperature of the catalysts. The fuels and air stream were pumped into the steel chamber and mixed well at 220 °C in the first heating zone. The second heating zone was maintained at 240 °C to prevent condensation of the evaporating gas mixture.

Within the third heating zone, the loaded catalyst was preheated and the temperature was 400 °C.

The results were analyzed by the gas chromatograph (Agilent GC 7890A). Two six-port valves were served to inject the sample of the produced effluents into the injection port of GC equipped with a molecular sieve column (30 m 0.32 mm ID, MOL SIV 5A, carrier gas = Ar) on a flame-ionization detector and a micro-packed column on a thermal-conductivity detector. A column (molecular sieve 5A) separated CH_4, C_2H_4, C_2H_5OH, and $C_xH_yO_z$, and a micro-packed column separated H_2, CO, and CO_2.

3. Results and discussion

3.1. Synthesis and characterization

3.1.1. Preparation of $La_2Ce_{2-x}Ru_xO_7$ solid solution

Pyrochlore phase $La_2Ce_2O_7$ was chosen as the host material; the B-site cations (Ce^{4+}) were substituted with the catalytically active Ru ions at varied concentration. According to the PXRD pattern (Fig. 1(a)), a solid solution of $La_2Ce_{2-x}Ru_xO_7$ resulted for $x = 0$–0.5 and an impure phase (RuO_2) formed for $x > 0.5$. The effect of the doped Ru^{4+} ions on the crystal unit cell is shown in Fig. 1(b) as a function of the cell volume versus molar ratio of Ru. The results indicate that the cell dimension is gradually decreased from 1394.04(1) to 1351.06(2) Å^3 and exhibits a linear relation in the range $x = 0$–0.35. The results of PXRD analyses indicate that the phase width of the solid solution $La_2Ce_{2-x}Ru_xO_7$ is in the range $x = 0$–0.35. Other properties including crystal size, specific surface area, and EDS of the materials as prepared are summarized in Table 1. The crystal sizes were estimated with the Scherrer equation; the average particle size decreased significantly from 25 to 11 nm when the Ru content was increased above 0.15. The crystal size and morphology that were investigated with the SEM (Fig. 2) indicate aggregated nanoparticles for all samples. The specific surface area of the materials as-prepared was measured and estimated with the Barrett-Emmett–Teller method; the values of all samples were within a small range 5–19 m^2/g. The small S_{BET} values reflect the high temperature of calcination under which most pore structures are collapsed [31].

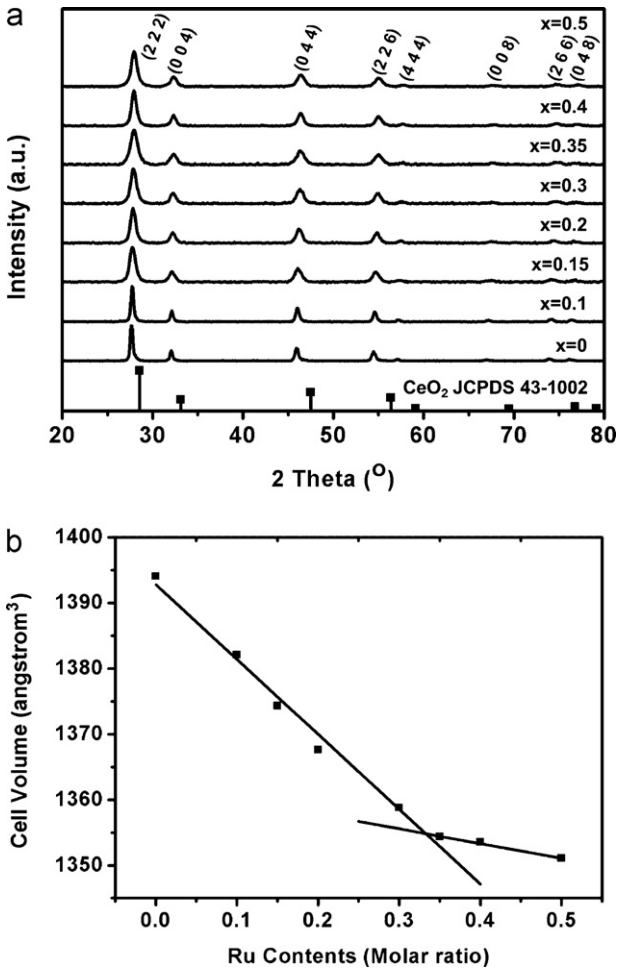

Fig. 1. Phase identification of $La_2Ce_{2-x}Ru_xO_7$ ($x = 0$–0.35); (a) powder X-ray diffraction; (b) cell refinement.

3.1.2. X-ray photoelectron spectra

Analysis of X-ray photoelectron spectra (XPS) was utilized to understand the oxidation states and defects in the materials as synthesized. The XPS spectra revealed characteristic features of Ce3*d* and Ru3*d* (Figure S1). The spectra of Ce3*d* were fitted to calculate the % (U''') value for semi-quantifying the fraction of Ce^{4+} in the as-prepared samples (Table S1) [11]. For undoped phase $La_2Ce_2O_7$, the calculated U''' value is 12.6 and the maximum value is observed for the sample of $x = 0.2$ ($U''' = 14.3$). For compounds with $x > 0.2$, the observed values of % (U''') are within 13.3–13.7. The results indicate that the relative amount of Ce^{4+} increased as the content of doped Ru increased until $x = 0.2$. The spectra of Ru3*d* were also fitted to understand the effect of Ru-doping to the oxidation state of Ce ions. The binding energies (BE) of Ru3$d_{5/2}$ were found in a range 281.66–282.99 eV (Table 2). For $x \leq 0.15$, only one XPS line was observed, but for $x > 0.15$ another line with a greater BE was also observed. According to the literature, the Ru3$d_{5/2}$ signal of Ru^{4+} is located in the range 280.7–281.0 eV and those of the highly oxidized RuO_x are assigned at 282.5–282.6 eV and 283.3 eV for RuO_3 and RuO_4, respectively [29]. The oxidation state of Ru in $La_2Ce_{2-x}Ru_xO_7$ is thus deduced as +4; there might exist some Ru ions with oxidation numbers >+4 in the samples with $x > 0.15$. This condition is reasonable because the calcination temperature 900 °C favors the formation of highly oxidized Ru ions [29]. Moreover, our BE of Ru ions are larger than those reported, which might be due to the metal–metal interaction between Ru and La/Ce ions. Fig. 3 shows the La3*d* spectra of the samples as prepared. The characteristic spectrum of La3*d* exhibits two asymmetric lines at ~839 (La3$d_{5/2}$) and ~856 eV (La3$d_{3/2}$) with their satellites at the smaller BE side as a shoulder, separately [32]. Four XPS lines are assigned as 3$d_{5/2}$ and 3$d_{3/2}$ levels for $La_2Ce_{2-x}Ru_xO_7$ ($x = 0$–0.35). Lines of ~838 (La3$d_{5/2}$) and ~855 eV (La3$d_{3/2}$) with their satellites at ~834 and ~851 eV, respectively, are assigned to the BE of La^{3+} in pyrochlore phase. The weak XPS lines centered at ~836 and ~853 eV with their satellites at lower energies of ~833 and ~849 eV, indicate partially reduced La ions.

Combining with the fitted results of XPS spectra, the correlation between Ce and Ru ions was proposed as follows. When the $La_2Ce_2O_7$ was doped with Ru, the unit cell dimension was reduced and favored for the small ionic radius Ce^{4+} ions. The oxidation state of Ru was +4 when $x < 0.2$. As the Ru content was increased, higher oxidation state of Ru^{n+} ($n > 4$) started to form and the La^{3+} and Ce^{4+} ions in the host material were partially reduced, which led to the formation of Ce^{+3} ions. The oxidation states of La were also affected by the doped-Ru element. The results of XPS analyses suggested that there were different kinds of environments for La ions on the surface of Ru-doped pyrochlore phase. The degree of disorder or metal-metal interaction increased, which led to the increased amount of partially reduced La ions. The maximum amount of Ce^{4+} was observed at $x = 0.2$. We proposed that a metal-metal interaction between Ru and La/Ce ions might exist due to the facts of greater BE for Ru ions than those reported and a smaller BE near the regular La^{3+} ions.

Table 1
Unit cell parameter, crystal size, Ru molar contents, and BET surface area of the solid solution $La_2Ce_{2-x}Ru_xO_7$ (x = 0–0.35).

x	0	0.1	0.15	0.2	0.3	0.35
Unit cell parameter/Å	11.171(4)	11.139(6)	11.118(3)	11.100(8)	11.076(3)	11.064(5)
Crystal size/nm[a]	25.77	25.78	11.73	13.07	11.84	9.90
Ru contents (molar ratio)[b]	N/A	0.06	0.13	0.20	0.29	0.34
Surface area/m^2g^{-1}	5.47	5.47	<2	2.84	18.66	19.29

[a] Calculate from PXRD pattern by Scherrer equation
[b] Calculate from EDS results

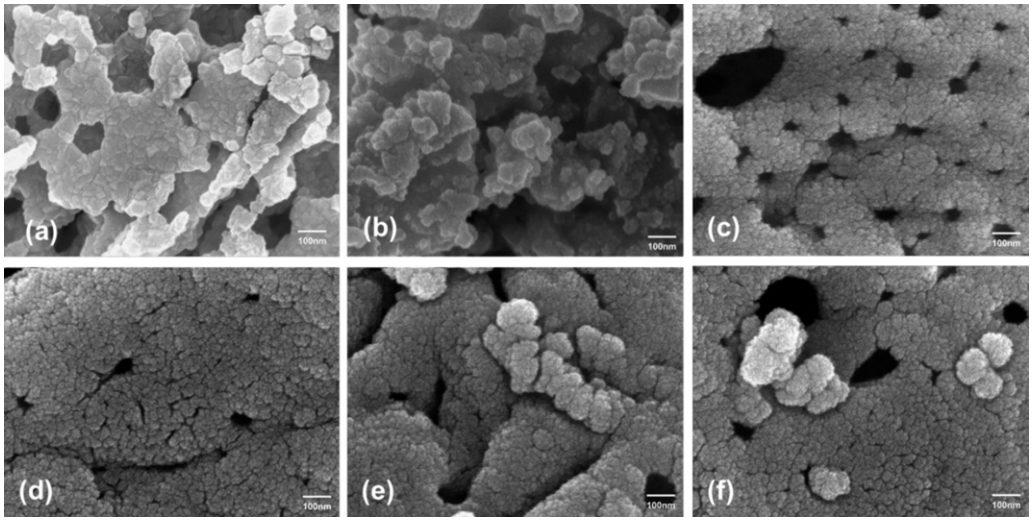

Fig. 2. SEM images of solid solution $La_2Ce_{2-x}Ru_xO_7$ (a) x = 0; (b) x = 0.1; (c) x = 0.15; (d) x = 0.2; (e) x = 0.3; (f) x = 0.35.

3.1.3. H_2 reduction ability

The reduction behavior of $La_2Ce_{2-x}Ru_xO_7$ (x = 0–0.35) as prepared was examined with a temperature-programmed reduction (TPR) system to investigate their catalytic properties; the TPR profiles appear in Fig. 4a. The reduction of Ru ions contribute to the temperature region <350 °C that are assigned to one or two lines. In the region >350 °C, reduction features of Ce^{4+} ions were observed. Doping with Ru ions seems to stabilize the B site in the structure of $La_2Ce_2O_7$ and the curves of H_2 consumption show a sustained reduction behavior after 350 °C. In $La_2Ce_2O_7$, reduction of the Ce^{4+} ions began at 400 °C and ended at 700 °C. For Ru-doped samples, two reduction features were observed for the reduction of $Ru^4 \rightarrow Ru^{3+}$ and $Ru^{3+} \rightarrow Ru^{2+}/Ru^0$. In addition, the reduction temperature of Ru ions was gradually shift to lower temperature, which is correlated with the shift of BE values for Ru ions (Table 2). As the proportion of Ru increased to x = 0.3 and 0.35, only one broad reduction line centered at 117 °C was observed, indicative of the existence of highly oxidized Ru ions in the solid solution as prepared; this result is consistent with the analysis of XPS.

Hydrogen consumption rates were calculated and depicted as a function of rate versus Ru content (Fig. 4b). Full reduction process was estimated in the temperature range of 60–900 °C. For ternary phase of $La_2Ce_2O_7$ (x = 0), H_2 consumption rate is 786 μmol/g. The reduction ability for Ru-doped samples is enhanced due to the effect from the defect formation when the B-site Ce ions are partially replaced by Ru ions. The highest H_2 consumption rate is 2714 μmol/g for $La_2Ce_{1.8}Ru_{0.2}O_7$.

Contributions of Ru and Ce ions in host material are evaluated by integration of hydrogen consumption in two parts, 60–350 for Ru and 350–900 °C for host materials, respectively. For the contributions of Ru ions, the H_2 consumption was increased gradually up to x = 0.15 and became stable between x = 0.15 and 0.30, finally the H_2 consumption increased to the higher rates at x = 0.35. For that of Ce ions, the H_2 consumption rate was first increased and stable at x = 0.1 and 0.15 (~1500 μmol/g); then reached to the maximum value of 2009 μmol/g at x = 0.2. As the amount of Ru ions increased

Table 2
Assignment of Ru3$d_{3/2}$ XPS lines of solid solution $La_2Ce_{2-x}Ru_xO_7$ (x = 0–0.35).

x	0	0.1	0.15	0.2	0.3	0.35
Ru3$d_{3/2}$	N/A	281.66	281.86	281.91	281.91	281.87
	N/A	N/A	N/A	282.98	282.99	282.95

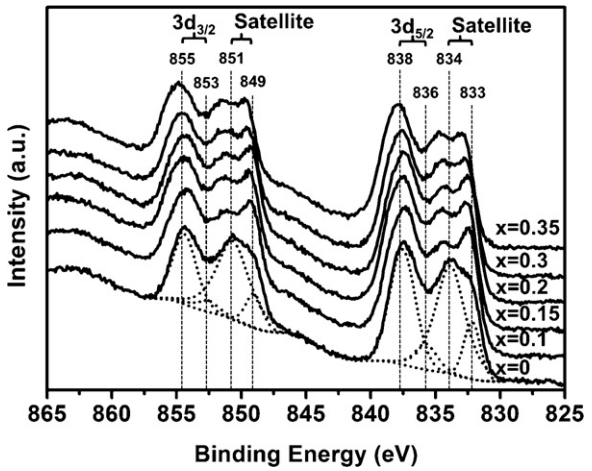

Fig. 3. La3d X-ray photoelectron spectra of $La_2Ce_{2-x}Ru_xO_7$ (x = 0–0.35). The marked lines are the uncommon split lines.

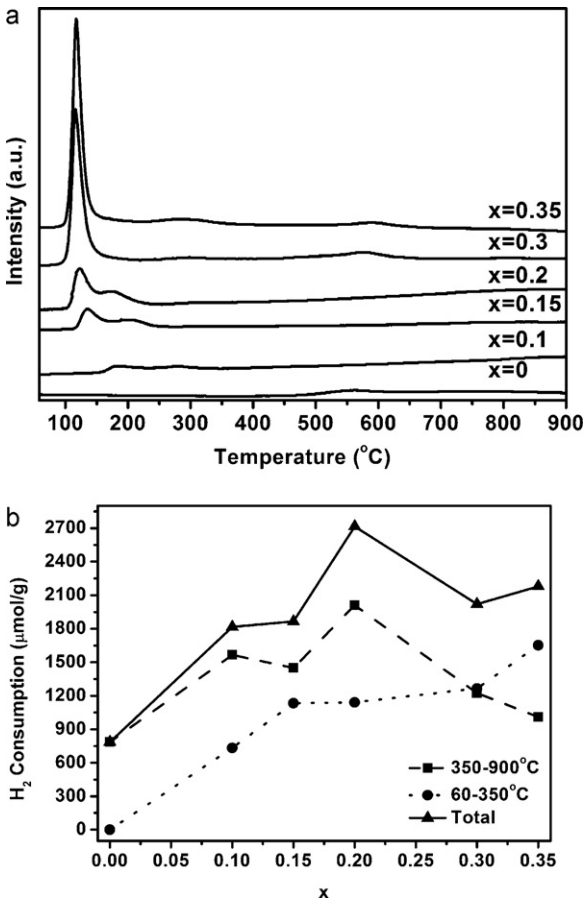

Fig. 4. (a) Temperature-programmed reduction profiles; (b) H_2 consumption of $La_2Ce_{2-x}Ru_xO_7$ (x = 0–0.35).

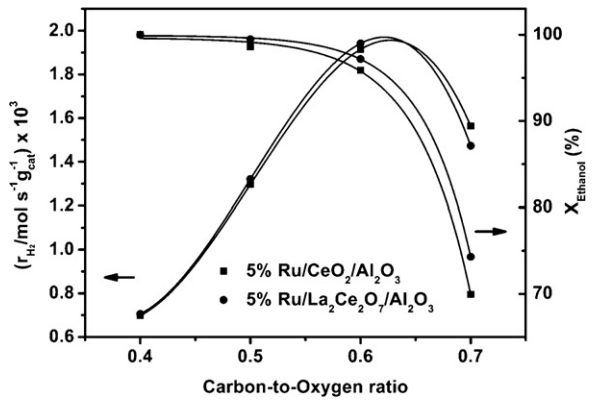

Fig. 5. H_2 production rate of catalysts, 5% Ru/CeO_2, and 5% $Ru/La_2Ce_2O_7$. (H_2O/ethanol = 3, GHSV = 1.6×10^5 h^{-1}, T = 400 °C).

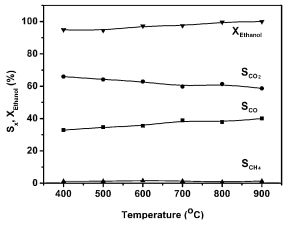

Fig. 6. Ethanol conversion and C-species selectivity as a function of reaction temperature. (Catalyst: $La_2Ce_{1.8}Ru_{0.2}O_7$; H_2O/ethanol = 3, GHSV = 1.6×10^5 h^{-1}, T = 400 °C, C/O = 0.4).

(x > 0.3), the H_2 consumption rate decreased. The trend of hydrogen consumption rate for Ce ions is similar to that of the total hydrogen consumption.

3.2. Catalytic performance

3.2.1. Performance of 5% Ru/CeO_2 and 5% $Ru/La_2Ce_2O_7$

CeO_2 is known as an efficient catalyst for the autothermal steam reforming of ethanol [6,33]. CeO_2 and host material $La_2Ce_2O_7$ were thus prepared through the same sol–gel method and served as a catalyst at 5% Ru loading for comparison. The performance in autothermal steam reforming of ethanol was tested to confirm the catalytic activity of CeO_2 and $La_2Ce_2O_7$. The corresponding r_{H_2} is shown in Fig. 5 (detailed results are summarized in Fig. S2); the catalyst, 5% $Ru/La_2Ce_2O_7$, reveals greater r_{H_2} than the 5% Ru/CeO_2 catalyst. Thus, $La_2Ce_2O_7$ is suitable for use as a host material not only because of the structural features but also the superior catalytic activity.

3.2.2. Performance of $La_2Ce_{2-x}Ru_xO_7$ (x = 0.1–0.35) solid solution

3.2.2.1. Effect of reaction temperature. The effect of temperature on autothermal steam reforming of ethanol was measured under the condition with carbon-to-oxygen ratio (C/O) of 0.4 and the corresponding total flow rate was 1.6×10^5 h^{-1} GHSV. The results displayed in Fig. 6 shows the corresponding conversion rate of ethanol ($X_{ethanol}$) and selectivities of C-species (S_x; x = CO, CO_2, CH_4). In general, an autothermal steam reforming reaction starts at T – 400 °C and the $X_{ethanol}$ reaches to a high value (≥95%). Change of distribution of products was observed with the increased temperature that S_{CO} slightly increased and S_{CO_2} decreased. This is due to the slightly endothermic enthalpy (ΔH_R = +20 kJ.mol) of partial oxidation reaction of ethanol. The results indicate that the effect of temperature is not obvious and the following measurements were all controlled at 400 °C.

3.2.2.2. Effect of carbon-to-oxygen ratio. The AESR performance was tested for the solid solution $La_2Ce_{2-x}Ru_xO_7$ (x = 0.1–0.35) supported on Al_2O_3. The C/O composition was varied from 0.4 to 0.7 to evaluate the catalytic activity of the catalysts as prepared with the preheating temperature controlled at 400 °C. Besides the production of gaseous H_2, CO, CO_2 and CH_4 (in trace proportion), no other CH_x species was detected with GC in all tests. The resulting catalytic performances are shown in Fig. 7, including ethanol conversion ($X_{ethanol}$), hydrogen production rate (r_{H_2}) and selectivities of C species (S_{CO} and S_{CO_2}). The C/O composition is a crucial factor in AESR reactions that dominate the contribution of the total and partial oxidations; the optimized value varies with the catalyst used. For all catalysts, r_{H_2} and S_{CO} increase with increasing C/O, but the opposite trend was found for S_{CO_2}. These results support that the total oxidation is favored at a small C/O level (high O_2 partial pressure) with production of CO_2, H_2O and much heat. The partial oxidation that produced CO and H_2 became predominant at a large C/O level (low O_2 partial pressure); r_{H_2} and S_{CO} increased and S_{CO_2} decreased. At C/O = 0.7, the incomplete conversion of ethanol was observed; $X_{ethanol}$ < 90%. The suppression of the water-gas-shift (WGS) reaction was concurrently observed, and S_{CO}/S_{CO_2} for all catalysts increased with the increasing C/O. This effect might be due to the high preheating temperature that is unfavorable for the exothermic WGS reaction.

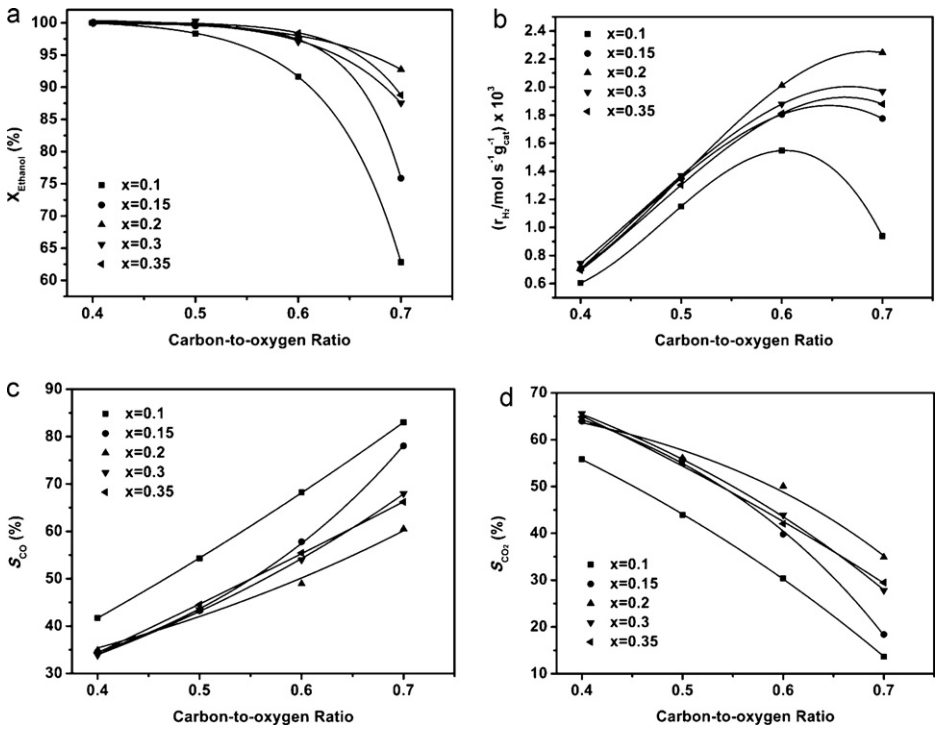

Fig. 7. Performance in autothermal steam reforming of ethanol with $La_2Ce_{2-x}Ru_xO_7$ (x = 0–0.35) according to (a) H_2 production rate; (b) ethanol conversion rate; (c) CO selectivity; (d) CO_2 selectivity. (H_2O/ethanol = 3, GHSV = 1.6×10^5 h^{-1}, T = 400 °C).

3.2.2.3. Effect of Ru doping. The effect of Ru doping to r_{H_2}, S_{CO} and S_{CO_2} was examined. For catalysts with $x \leq 0.3$, r_{H_2} gradually increased with an increasing proportion of Ru, but greater Ru doping led to a restrained yield of H_2. The variations of S_{CO} and S_{CO_2} were monitored to consider possible routes of the reaction. As the Ru proportion was increased from x = 0.1 to 0.3, S_{CO} decreased, accompanied by increased S_{CO_2}. S_{CO}/S_{CO_2} also decreased significantly with increasing Ru in a solid solution, especially at a large C/O level. Possible explanations of these results follow. (1) The Ru-doped $La_2Ce_2O_7$ structure might enhance the WGS reaction that leads to enhanced H_2 production and the elimination of residual CO. (2) The conversion rate of ethanol at C/O = 0.7 was improved on Ru doping; an increased $X_{ethanol}$ value is observed in Fig. 6(a). The optimized catalyst on an AESR reaction is $La_2Ce_{1.8}Ru_{0.2}O_7$ which, with the great $r_{H_2} = 0.70 \sim 2.24 \times 10^{-3}$ mol s^{-1} $gcat^{-1}$, gives the smallest yield of harmful gas CO and a rate of conversion of ethanol >90%. Several materials were investigated as catalysts on AESR reaction and their corresponding rates (r_{H_2}) were estimated from given data. For Rh-based catalyst, the 5% Rh/CeO_2 revealed the $r_{H_2} \sim 1.18 \times 10^{-3}$ mol s^{-1} $gcat^{-1}$ under a gas flow rate (GHSV $\sim 1 \times 10^5$ h^{-1}) [6]. Under a similar flow rate to this work, a better $r_{H_2} = 2.88 \times 10^{-3}$ mol s^{-1} $gcat^{-1}$ was observed. The drawback for Rh-based catalysts is their cost [6,33]. For low-cost Ni-based catalysts, the ease of oxidation and coke deposition of Ni metal made Ni-based catalysts not stable during the AESR reaction, which were mostly applied under a low flow rate (GHSV ~ 10,000 h^{-1}) [34,35]. The catalyst 20% Ni/ZrO_2 exhibited the rate $r_{H_2} = 3.73 \times 10^{-4}$ mol s^{-1} $gcat^{-1}$ [35]. The reduced $LaNiO_3$ was prepared to prevent the deactivation of Ni metal and it showed $r_{H_2} = 1.7 \times 10^{-3}$ mol s^{-1} $gcat^{-1}$ [34]. The as-prepared $La_2Ce_{1.8}Ru_{0.2}O_7$ exhibits high activity on AESR reaction compare to these catalysts.

3.2.2.4. The effect of preparation route. From the results of the AESR performance, the catalyst 5% $Ru/La_2Ce_2O_7$ shows a slightly greater r_{H_2} than that of 5% Ru/CeO_2, which indicates that $La_2Ce_2O_7$ is

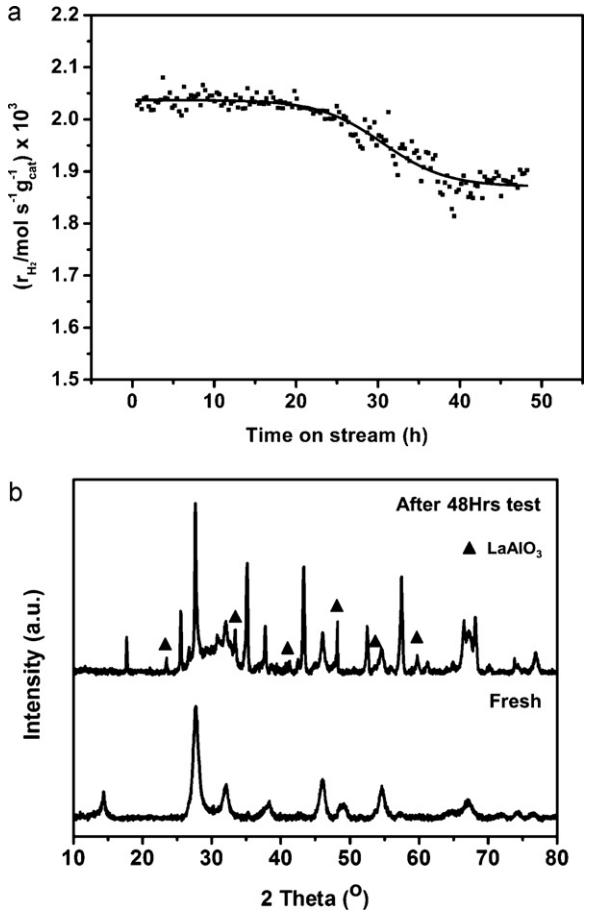

Fig. 8. Stability test of $La_2Ce_{1.8}Ru_{0.2}O_7$. (a) H_2 production rate; (b) powder X-ray diffraction before and after 48 h test. (H_2O/ethanol = 3, GHSV = 1.6×10^5 h^{-1}, T = 400 °C, C/O = 0.6).

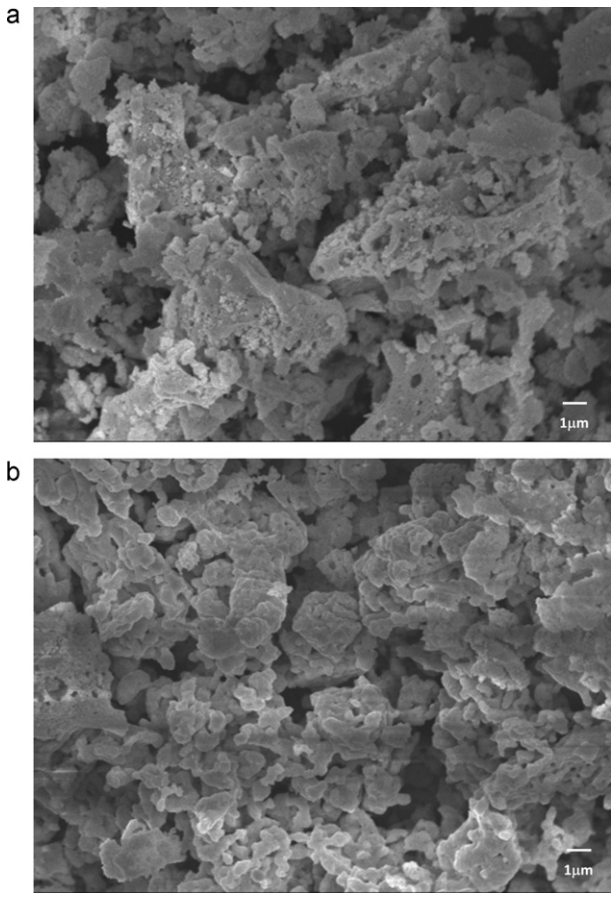

Fig. 9. SEM images (a) before and (b) after the stability test.

suitable to serve as the host material. Taking the molar ratio of Ru/Ce loading into consideration, the values, 0.085, 0.166 and 0.111 correspond to the Ru/Ce values of 5% Ru/CeO_2, 5% Ru/$La_2Ce_2O_7$, and $La_2Ce_{1.8}Ru_{0.2}O_7$, respectively. Although CeO_2 and $La_2Ce_2O_7$ revealed similar reductive ability in TPR experiments, the slightly greater r_{H_2} of 5% Ru/$La_2Ce_2O_7$ (Ru/Ce = 0.166) might be due to the greater molar ratio of Ru/Ce loading. Furthermore, the greatest r_{H_2} was observed for the catalyst $La_2Ce_{1.8}Ru_{0.2}O_7$ containing the molar ratio Ru/Ce = 0.111. Compared with the catalyst 5% Ru/$La_2Ce_2O_7$, the molar ratio of Ru/Ce loading was decreased without deteriorating the AESR performance for the catalyst $La_2Ce_{1.8}Ru_{0.2}O_7$. This result correlates to the effective distribution of Ru ions in the solid solution $La_2Ce_{1.8}Ru_{0.2}O_7$. The synthesis of the solid solution is therefore expected to be a superior way to prepare highly efficient catalysts.

3.2.2.5. Stability test of $La_2Ce_{1.8}Ru_{0.2}O_7$. We tested the enduring catalytic stability of $La_2Ce_{1.8}Ru_{0.2}O_7$ at C/O = 0.6. As shown in Fig. 8(a), the r_{H_2} degraded about 5–10% after a 48 h experiment. The PXRD patterns were collected before and after the stability test and are shown in Fig. 8(b). The pattern of the used catalyst shows that a new phase, $LaAlO_3$, began to form, and a decreased FWHM of $La_2Ce_{1.8}Ru_{0.2}O_7$ was observed, indicative of phase decomposition and particle aggregation, respectively. The crystalline phase of the support Al_2O_3 also altered from corundum to α-, δ-, κ-phase, which affected the catalytic routes and led to the degradation of H_2 production. The SEM images of the fresh and used catalysts are shown in Fig. 9. The results indicate the destruction of the pore structure and the melting-like morphology after the protracted AESR experiment. These results are consistent with the crystallinity change in PXRD patterns. The distribution of Ru ions on the catalyst $La_2Ce_{1.8}Ru_{0.2}O_7$ before and after the AESR reaction was tested using TEM element-mapping analysis (Fig. S3). The mapping images showed an even dispersion of Ru ions in both samples, which indicated that, the preparation of a solid solution was an effective method to prevent the aggregation of active metals. The ICP-AES analyses were taken on the fresh and used catalysts. As shown in Table S2, no obvious change on Ru composition was observed, which indicated that the amount of Ru in the as-prepared catalyst did not lost during the ethanol reforming process.

4. Conclusion

$La_2Ce_{2-x}Ru_xO_7$ (x = 0–0.5) solid solutions were prepared through the sol–gel method; the pure phases had x = 0–0.35. The XPS analyses indicate that most Ru is in oxidation state +4; highly oxidized Ru ions exist in samples with x > 0.15. A metal–metal interaction occurs between Ru and La ions, leading to the formation of partially reduced La ions. From the TPR profiles, the reduction temperatures of Ru and Ce ions shift to higher and lower temperatures, respectively, because of this metal–metal interaction. According to tests of the AESR performance, the optimized catalyst is $La_2Ce_{1.8}Ru_{0.2}O_7$ with the r_{H_2}, 2.01×10^{-3} mol s^{-1} g_{cat}^{-1} at C/O = 0.6 ($X_{ethanol}$ > 95%). The enduring stability was tested on $La_2Ce_{1.8}Ru_{0.2}O_7$; the r_{H_2} degraded about 5–10% after 48 h. The major problem would be the reaction between $La_2Ce_{1.8}Ru_{0.2}O_7$ and the Al_2O_3 support.

Acknowledgements

National Science Council (NSC98-2113-M-009-007-MY3, 99-3113-P-009-005) and Center for Green Energy Technology supported this work.

Appendix A. Supplementary data

Supplementary data associated with this article can be found, in the online version, at http://dx.doi.org/10.1016/j.apcatb.2013.01.025.

References

[1] D. Das, T.N. Veziroglu, International Journal of Hydrogen Energy 26 (2001) 13–28.
[2] J.P.W. Scharlemann, W.F. Laurance, Science 319 (2008) 43–44.
[3] A. Haryanto, S. Fernando, N. Murali, S. Adhikari, Energy Fuels 19 (2005) 2098–2106.
[4] M. Ni, D.Y.C. Leung, M.K.H. Leung, International Journal of Hydrogen Energy 32 (2007) 3238–3247.
[5] J. Xuan, M.K.H. Leung, D.Y.C. Leung, M. Ni, Renewable and Sustainable Energy Reviews 13 (2009) 1301–1313.
[6] G.A. Deluga, J.R. Salge, L.D. Schmidt, X.E. Verykios, Science 303 (2004) 993–997.
[7] F. Lenormand, L. Hilaire, K. Kili, G. Krill, G. Maire, Journal of Physical Chemistry 92 (1988) 2561–2568.
[8] J. Stubenrauch, J.M. Vohs, Journal of Catalysis 159 (1996) 50–57.
[9] J. Kaspar, P. Fornasiero, M. Graziani, Catalysis Today 50 (1999) 285–298.
[10] K.B. Zhou, X. Wang, X.M. Sun, Q. Peng, Y.D. Li, Journal of Catalysis 229 (2005) 206–212.
[11] A. Trovarelli, Catalysis by Ceria and Related Materials, 2nd. ed., Imperial College, London, 2002.
[12] W.I. Hsiao, Y.S. Lin, Y.C. Chen, C.S. Lee, Chemical Physics Letters 441 (2007) 294–299.
[13] Y.C. Chen, K.B. Chen, C.S. Lee, M.C. Lin, Journal of Physical Chemistry C 113 (2009) 5031–5034.
[14] W.T. Chen, K.B. Chen, M.F. Wang, S.F. Weng, C.S. Lee, M.C. Lin, Chemical Communication 46 (2010) 3286–3288.
[15] J.B. Thomson, A.R. Armstrong, P.G. Bruce, Journal of Solid State Chemistry 148 (1999) 56–62.
[16] H. Kishimoto, T. Omata, S. Otsuka-Yao-Matsuo, K. Ueda, H. Hosono, H. Kawazoe, Journal of Alloys and Compounds 312 (2000) 94–103.
[17] D.J. Haynes, D.A. Berry, D. Shekhawat, J.J. Spivey, Catalysis Today 136 (2008) 206–213.
[18] S. Gaur, D.J. Haynes, J.J. Spivey, Applied Catalysis A: General 403 (2011) 142–151.

[19] T. Montini, M.A. Banares, N. Hickey, R. Di Monte, P. Fornasiero, J. Kaspar, M. Graziani, Physical Chemistry Chemical Physics 6 (2004) 1–3.
[20] T. Montini, N. Hickey, P. Fornasiero, M. Graziani, M.A. Banares, M.V. Martinez-Huerta, I. Alessandri, L.E. Depero, Chemistry of Materials 17 (2005) 1157–1166.
[21] P.R. Shah, T. Kim, G. Zhou, P. Fornasiero, R.J. Gorte, Chemistry of Materials 18 (2006) 5363–5369.
[22] R. Kieffer, M. Fujiwara, L. Udron, Y. Souma, Catalysis Today 36 (1997) 15–24.
[23] J.M. Sohn, M.R. Kim, S.I. Woo, Catalysis Today 83 (2003) 289–297.
[24] D.J. Haynes, D.A. Berry, D. Shekhawat, J.J. Spivey, Catalysis Today 145 (2009) 121–126.
[25] K. Matsuhira, M. Wakeshima, Y. Hinatsu, S. Takagi, Journal of the Physical Society of Japan 80 (2011).
[26] M.G. Brik, A.M. Srivastava, N.M. Avram, Optical Materials 33 (2011) 1671–1676.
[27] K.A. Ross, L.R. Yaraskavitch, M. Laver, J.S. Gardner, J.A. Quilliam, S. Meng, J.B. Kycia, D.K. Singh, T. Proffen, H.A. Dabkowska, B.D. Gaulin, Physical Review B 84 (2011).
[28] J.K. Gill, O.P. Pandey, K. Singh, Solid State Science 13 (2011) 1960–1966.
[29] L. Ji, J. Lin, H.C. Zeng, Chemistry of Materials 13 (2001) 2403–2412.
[30] J.R. Salge, G.A. Deluga, L.D. Schmidt, Journal of Catalysis 235 (2005) 69–78.
[31] J. Lee, M.C. Orilall, S.C. Warren, M. Kamperman, F.J. Disalvo, U. Wiesner, Natural Materials 7 (2008) 222–228.
[32] B.V. Kumar, R. Velchuri, V.R. Devi, B. Sreedhar, G. Prasad, D.J. Prakash, M. Kanagaraj, S. Arumugam, M. Vithal, Journal of Solid State Chemistry 184 (2011) 264–272.
[33] W.J. Cai, F.G. Wang, A.C. Van Veen, H. Provendier, C. Mirodatos, W.J. Shen, Catalysis Today 138 (2008) 152–156.
[34] H.Q. Chen, H. Yu, F. Peng, G.X. Yang, H.J. Wang, J. Yang, Y. Tang, Chemical Engineering Journal 160 (2010) 333–339.
[35] M.H. Youn, J.G. Seo, J.C. Jung, S. Park, D.R. Park, S.B. Lee, I.K. Song, Catalysis Today 146 (2009) 57–62.